ACS NANO
Cite This: ACS Nano 2017, 11, 12780–12788
www.acsnano.org

ARTICLE

Toward a Mechanistic Understanding of Vertical Growth of van der Waals Stacked 2D Materials: A Multiscale Model and Experiments

Han Ye,[†,‡] Jiadong Zhou,[§] Dequan Er,[‡] Christopher C. Price,[‡] Zhongyuan Yu,[†] Yumin Liu,[†] John Lowengrub,[⊥] Jun Lou,[∥] Zheng Liu,[§] and Vivek B. Shenoy*[,‡]

[†]State Key Laboratory of Information Photonics and Optical Communications, Beijing University of Posts and Telecommunications, Beijing 100876, China

[‡]Department of Materials Science and Engineering, University of Pennsylvania, Philadelphia, Pennsylvania 19104, United States

[§]Centre for Programmable Materials, School of Materials Science and Engineering, Nanyang Technological University, Singapore 639798, Singapore

[⊥]Departments of Mathematics and Chemical Engineering & Materials Science, University of California, Irvine, California 92697, United States

[∥]Department of Materials Science and NanoEngineering, Rice University, Houston, Texas 77005, United States

Supporting Information

Vertical stacking of monolayers *via* van der Waals (vdW) interaction opens promising routes toward engineering physical properties of two-dimensional (2D) materials and designing atomically thin devices. However, due to the lack of mechanistic understanding, challenges remain in the controlled fabrication of these structures *via* scalable methods such as chemical vapor deposition (CVD) onto substrates. In this paper, we develop a general multiscale model to describe the size evolution of 2D layers and predict the necessary growth conditions for vertical (initial + subsequent layers) *versus* in-plane lateral (monolayer) growth. An analytic thermodynamic criterion is established for subsequent layer growth that depends on the sizes of both layers, the vdW interaction energies, and the edge energy of 2D layers. Considering the time-dependent growth process, we find that temperature and adatom flux from vapor are the primary criteria affecting the self-assembled growth. The proposed model clearly demonstrates the distinct roles of thermodynamic and kinetic mechanisms governing the final structure. Our model agrees with experimental observations of various monolayer and bilayer transition metal dichalcogenides grown by CVD and provides a predictive framework to guide the fabrication of vertically stacked 2D materials.

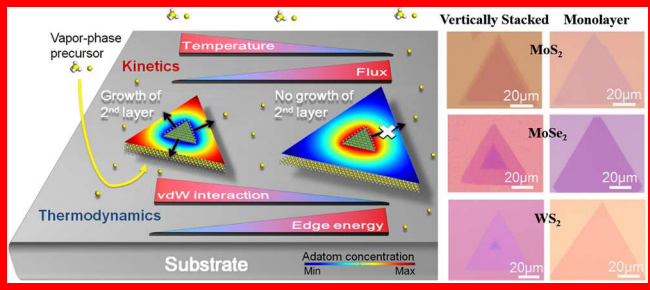

vertically stacked 2D materials, growth mechanisms, thermodynamic criterion, kinetic models, transition metal dichalcogenides, chemical vapor deposition

Two-dimensional (2D) materials including group IV, group V, group III-V compounds, and transition metal dichalcogenides (TMDs) have garnered significant interest in pursuit of appealing electronic, optical, mechanical, and thermal properties.[1−10] Recently, two or more monolayers vertically stacked *via* van der Waals (vdW) interaction have been successfully fabricated in experiments.[11−20] These structures further expand the possibility of physical property manipulation and the potential design space for atomically thin devices. For example, the capability to continuously tune the band gap using external electric fields emerges in both bilayer semiconducting MoS_2[11−13] and bilayer semimetal graphene,[14−16] making these structures highly desirable for field-effect transistor applications. More importantly, vertical stacking of 2D materials can lead to the creation of heterostructures for improved electronic and optoelectronic devices. Recent demonstrations of such device concepts include thin p−n junctions (*e.g.*, MoS_2/WSe_2),[17,18] structures with interlayer excitons (*e.g.*, $MoSe_2/WSe_2$),[19,20] rapid interlayer

Received: October 26, 2017
Accepted: December 5, 2017
Published: December 5, 2017

DOI: 10.1021/acsnano.7b07604
ACS Nano 2017, 11, 12780–12788

charge transfer (MoS_2/WS_2),[21−23] and efficient energy transfer (MoS_2/WS_2).[24]

Common fabrication techniques of vertically stacked 2D materials involve direct mechanical exfoliation from the bulk[25] or mechanical transfer of one individually grown monolayer onto another.[12,13] The major drawbacks of these techniques are limited scalability, lack of precise stacking orientation control, and contamination on the layer−layer interface. Bottom-up fabrication using chemical vapor deposition (CVD) is therefore widely regarded as a superior synthesis route[26−28] because it avoids these issues while allowing potential growth of in-plane lateral heterostructures by self-assembly. However, the CVD approach involves a complex growth environment with several degrees of freedom that will influence the final structure. Gong *et al.* recently reported one-step vapor phase growth of high-quality vertically stacked (at 1123 K) and in-plane lateral (at 923 K) WS_2/MoS_2 heterostructures on SiO_2/Si substrates.[26] The growth temperature was found to be responsible for the growth mode switching, and this effect was ascribed to the competition between kinetically and thermodynamically dominant mechanisms. Xia *et al.*[27] grew triangular MoS_2 bilayers at 1123 K on SiO_2/Si substrates, observing both the majority AA′[29] and minority AB stacking configurations. In this system, Shang *et al.*[30] have shown Mo diffusion to be the growth rate limiting factor and obtained a critical layer size of 9.2 nm × 9.2 nm for freestanding systems using density functional theory (DFT) calculations. Below this substrate-dependent critical layer size, the MoS_2 monolayer is thermodynamically preferable to the bilayer structure. In addition to temperature, the gas ratio of CH_4:H_2 in CVD has been demonstrated to influence bilayer growth of hexagonal graphene on the Cu(111) surface, with higher H_2 concentration favoring the bilayer[31−33] along with lower growth temperature.[34]

Based on the initial experimental efforts, determining proper growth parameters is clearly a multivariable problem that has so far been addressed with tedious trial and error approaches due to a lack of mechanistic understanding. Unfortunately, current theoretical models do not provide a clear interpretation of the competition between vertical and in-plane lateral growth of 2D materials. Hence, a predictive growth model that addresses thermodynamic and kinetic factors is highly desirable. In the present work, we propose a general multiscale model for CVD growth of vertically stacked 2D materials. We primarily aim to capture the underlying physics and interpret (i) the thermodynamic requirements for vertical growth, (ii) the time-dependent growth rate and size evolution of both layers, and (iii) the growth conditions relevant to experiments.

RESULTS AND DISCUSSION

The key ingredients of the general multiscale model developed for the growth of vertically stacked 2D materials on a substrate are depicted in Figure 1. Attachment and diffusion of adatoms lead to the layer growth after nucleation. To maintain generality, the initial layer and the newly growing layer are denoted as layer 1 (Layer1) and layer 2 (Layer2), respectively. A thermodynamic description of the system requires accounting for the following factors: (i) the energy change upon incorporation of adatoms into the growing 2D layers, (ii) the distinct vdW interactions between the 2D layers and between the substrate and the 2D layer, (iii) the energy penalty of layer edges, and (iv) the entropy of the adatoms. Taking these into consideration, the total free energy of the system is written as

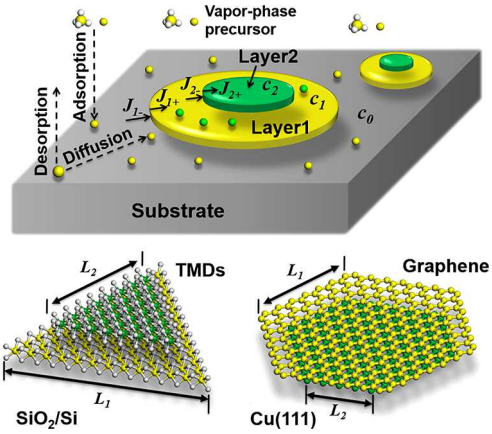

Figure 1. Schematic of the growth model for vertically stacked 2D materials. The variables c_n, J_n, and L_n (n = 0, 1, 2) are the adatom concentration in domain n, the flux of adatoms to the domain boundary, and the edge length of domain n, respectively.

$$E_{\text{free}} = S_2(-\varepsilon_2) + (S_1 - S_2)(-\varepsilon_1) + \Gamma_2\gamma_2 + \Gamma_1\gamma_1 + k_B T\int_0^\infty c[\ln(c/c_{\text{ref}}) - 1]\,\mathrm{d}S \quad (1)$$

where γ_n is the edge energy per unit length, S_n and Γ_n are the area and perimeter of the layers, c is the adatom concentration, and c_{ref} is the reference adatom concentration. The subscripts n = 0, 1, 2 refer to the substrate, layer 1, and layer 2, respectively. The binding energies per unit area of monolayer (ε_1) and bilayer (ε_2) account for in-plane bonding within the nucleated layers and any corresponding vdW interactions; these contributions are given by the first two terms. The third and fourth terms account for the energies of the growing edges, which are linearly dependent on the perimeters. The last term accounts for the entropy of the adatoms on both the substrate and 2D layers.

The size evolution of layer 1 and layer 2 is constrained by mass conservation, which ensures that layer growth is related to the net flux of adatoms diffusing to the boundary of each layer. This conservation law can be used to obtain the time dependence of the edge length (L_n):

$$\frac{\partial L_n}{\partial t} = \frac{\eta}{\Omega_s}(J_{n+} - J_{n-}),\ n = 1, 2 \quad (2)$$

where Ω_s is the concentration of atomic sites in the 2D layer. The structural parameter η is determined by the shape of the layers; $\eta = 2\sqrt{3}$ for an equilateral triangle and $\eta = 2/\sqrt{3}$ for an equilateral hexagon. Here, $J_{n\pm}$ are the diffusion fluxes of adatoms to the layer boundaries, with the "+" and "−" subscripts differentiating opposite sides of the boundary. In this convention, the "−" ("+") subscript describes the flux originating from the domain with the lower (same) n index (see Figure 1).

To determine the adatom fluxes to the layer edges based on the second law of thermodynamics, we next consider the variation of the total free energy with respect to time. By substituting $\partial L_n/\partial t$ using eq 2 and combining terms with similar boundary fluxes $J_{n\pm}$, this variation is expressed as

DOI: 10.1021/acsnano.7b07604
ACS Nano 2017, 11, 12780−12788

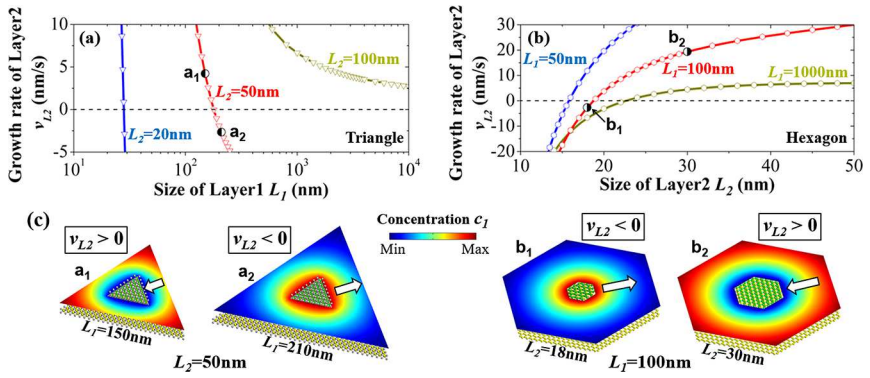

Figure 2. Relations between growth rate of layer 2 and layer sizes. (a) At fixed size of layer 2 (L_2) using triangular shape. (b) At fixed size of layer 1 (L_1) using hexagonal shape. (c) Profiles of adatom concentration on layer 1 (c_1) for the marked points in (a) and (b). The arrows indicate the directions of adatom diffusion.

$$\frac{\partial E_{\text{free}}}{\partial t} = \Gamma_1 J_{1+}\left(\frac{-\varepsilon_1}{\Omega_s} + \eta\frac{\gamma_1}{\Omega_s L_1} - \mu_{1+}\right) + \Gamma_1 J_{1-}\left(-\frac{-\varepsilon_1}{\Omega_s} - \eta\frac{\gamma_1}{\Omega_s L_1} + \mu_{1-}\right) + \Gamma_2 J_{2+}\left(\frac{\varepsilon_1 - \varepsilon_2}{\Omega_s} + \eta\frac{\gamma_2}{\Omega_s L_2} - \mu_{2+}\right) + \Gamma_2 J_{2-}\left(-\frac{\varepsilon_1 - \varepsilon_2}{\Omega_s} - \eta\frac{\gamma_2}{\Omega_s L_2} + \mu_{2-}\right) - D\int_0^\infty \frac{k_B T}{c}(\nabla c)^2\, \mathrm{d}S + \int_0^\infty \mu\left(F - \frac{c}{\tau_d}\right)\mathrm{d}S \quad (3)$$

Here, the chemical potential of the adatoms is defined as $\mu = k_B T \ln(c/c_{\text{ref}})$. The second law of thermodynamics stipulates that $\partial E_{\text{free}}/\partial t < 0$. This condition can be achieved if we choose $J_{n\pm}$ as

$$J_{1+} = K_{1+}\left(\frac{\varepsilon_1}{\Omega_s} - \eta\frac{\gamma_1}{\Omega_s L_1} + \mu_{1+}\right)$$
$$J_{1-} = K_{1-}\left(-\frac{\varepsilon_1}{\Omega_s} + \eta\frac{\gamma_1}{\Omega_s L_1} - \mu_{1-}\right)$$
$$J_{2+} = K_{2+}\left(\frac{\varepsilon_2 - \varepsilon_1}{\Omega_s} - \eta\frac{\gamma_2}{\Omega_s L_2} + \mu_{2+}\right)$$
$$J_{2-} = K_{2-}\left(-\frac{\varepsilon_2 - \varepsilon_1}{\Omega_s} + \eta\frac{\gamma_2}{\Omega_s L_2} - \mu_{2-}\right) \quad (4)$$

In these boundary conditions, $K_{n\pm}$ are kinetic coefficients accounting for the attachment/detachment of adatoms at the domain boundary n. The outward normal growth rate of layers can be estimated by $v_n = \frac{1}{\Omega_s L_n}\int_0^{L_n}(J_{n+} - J_{n-})\,\mathrm{d}l$. Finally, to quantitatively obtain the distributions of adatom concentration and the growth rates of 2D layers, n independent diffusion equations are constructed for n domains:

$$\frac{\partial c_n}{\partial t} = D_n \nabla^2 c_n + F_n - \tau_{d,n}^{-1} c_n \quad (5)$$

Here, D_n is the diffusion coefficient, F_n is the rate of adatom supply that accounts for adsorption rate and precursor decomposition, and τ_d is the effective lifetime of adatoms due to desorption. A diffusion length λ for the adatoms within their lifetime can be calculated using the relation $\lambda = \sqrt{D\tau_d}$. Equation 4 provides the flux boundary conditions for the corresponding nth diffusion equation in eq 5. The last boundary condition, $J_0 = 0$, accounts for the far-field condition at the edge of the substrate. The reference adatom concentration is taken to be $c_{\text{ref}} = F\tau_d$. In the calculations, we ignore the possibility of adatom adsorption and desorption on the top of 2D layers since the CVD precursors generally do not decompose/break down on these surfaces. Throughout the rest of paper, we have adopted the following default parameter set in numerical simulations for generality: $\lambda_n = 10\ \mu$m, $\tau_{d,0} = 10$ s, $F_0 = 10^{-3}\Omega_s$, $\Omega_s \approx 10^{20}$ m^{-2}, $\Delta\varepsilon_{\text{bind}} = 5$ meV/Å^2, $\varepsilon_1 = 20\Delta\varepsilon_{\text{bind}}$, $\varepsilon_2 = 2\varepsilon_1 + \Delta\varepsilon_{\text{bind}}$, $\gamma_n = 1$ eV/Å, $K_{n-} = 10K_{n+}$, and $T = 1000$ K.

The proposed model aims to capture the essential thermodynamics and kinetics of deposition-based 2D layered crystal growth while maintaining enough generality for major 2D material systems of interest. Bilayer growth in pure MoS_2 and WS_2/MoS_2 heterostructure systems has been experimentally observed to form stacked triangular layers as described in our model system.[26,27] For layer growth of TMDs, the diffusion of the adsorbed transition metal atoms (*e.g.*, Mo) has been shown to be the rate-limiting process due to much lower diffusivity[30] and lower concentration[27] than the chalcogen atoms. Therefore, in the present work, we focus on the diffusive mechanisms of only transition metal atoms, setting aside the detailed chemical reaction process[30] and the macroscopic shape evolution[35] of the 2D layers. This allows us to consider additional systems such as bilayer graphene, where the subsequent layer is inserted between the initial hexagonal layer and the Cu(111) surface.[31] The primary lateral diffusion mechanism of carbon adatoms to the subsequent layer involves hopping between the first subsurface sites in the Cu substrate,[32] and we can use our model without modification despite the positional change. The model does not include strain effects and the related defects induced by lattice mismatch and is therefore valid for heterostructure systems with similar lattice constants, such as TMDs with identical chalcogen atoms (*e.g.*, WS_2/MoS_2).

Larger (Smaller) Size of Initial (Subsequent) Layer Reduces the Growth Rate of Subsequent Layer, Even Prohibiting Growth. We obtain the growth rates of layer 1

DOI: 10.1021/acsnano.7b07604
ACS Nano 2017, 11, 12780−12788

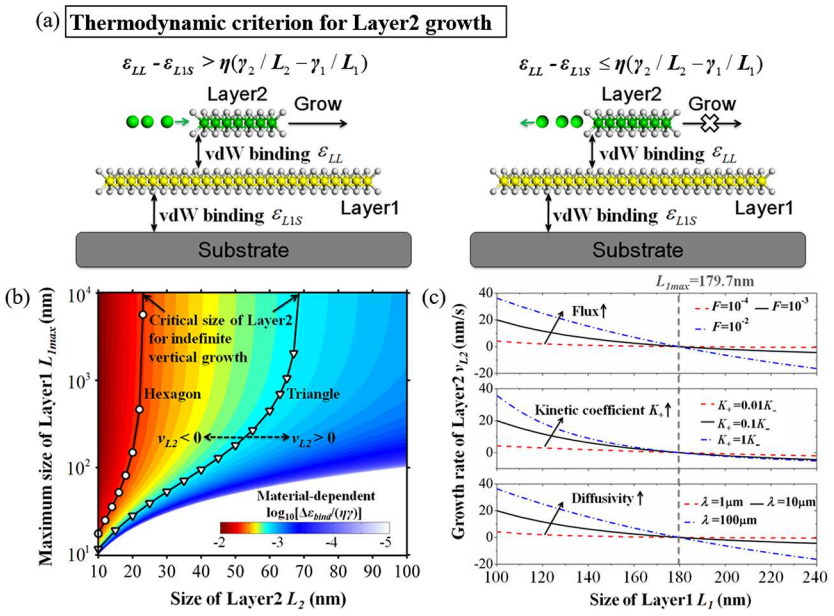

Figure 3. (a) Schematics for two scenarios based on the thermodynamic criterion for layer 2 growth (layer 2 on top of layer 1). (b) Heat map of the minimum required value of material-specific property $\Delta\varepsilon_{bind}/(\eta\gamma)$ to ensure vertical growth is thermodynamically favored (left scenario in (a)) at different sizes of layer 1 and layer 2. The solid lines with open symbols are obtained from numerical simulations of hexagonal and triangular bilayers which scan over the size limit L_{1max}. If the layer sizes fall to the right (left) side of the corresponding line for a certain material, growth of layer 2 is preferable (prohibited). (c) Influences of flux (unit Ω_s), kinetic coefficient, and diffusivity on the growth rate of layer 2, assuming a fixed layer 2 size of 50 nm. Other growth parameters are the same as those adopted in Figure 2.

and layer 2 and the adatom concentration profiles by numerically solving eq 5 with the boundary conditions described in eq 4. We find that the growth rate of layer 2 (v_{L2}) strongly depends on the sizes of layer 1 (L_1) and layer 2 (L_2), to the extent that size limits are observed that determine whether layer 2 will grow. As shown in Figure 2(a), for a given L_2, v_{L2} monotonically decreases with increasing L_1, even becoming negative at a maximum value L_{1max}, which indicates that layer 2 growth is prohibited. For example, for fixed L_2 of 20 and 50 nm, the crossover point L_{1max} is found at 28.1 and 179.7 nm, respectively; if L_1 exceeds these values, growth of layer 2 will cease. Correspondingly, if L_1 is fixed instead of L_2, v_{L2} monotonically increases with increasing L_2. We again observe negative v_{L2} values up until a certain minimum value L_{2min} as shown in Figure 2(b). This is analogous to a critical nucleation size that depends on L_1 for layer 2 growth. Therefore, we conclude that for a certain size of layer 2 (layer 1), there exists a maximum (minimum) size of layer 1 (layer 2) to ensure vertical growth, and decreasing the size difference between the two layers benefits bilayer growth. This phenomenon is observed in all studied layer shapes. The adatom concentration profiles on layer 1 match this behavior as illustrated in Figure 2(c); adatoms diffuse toward (away) from layer 2 if the vertical growth is preferable (prohibited).

An Analytic Thermodynamic Criterion Involving the vdW Interaction Energies and the Edge Energies Determines Whether the Subsequent Layer Can Grow at a Particular Size. To explicitly determine the requirements for the growth of layer 2, we consider the flux boundary conditions in eq 4, which ensure the evolution of the system is thermodynamically favorable. In the limiting case of K_{n-} approaching infinity (which corresponds to fast attachment), the adatom concentrations on the boundaries of layer 1 and layer 2 are expressed as $c_{1-} = c_{ref}\exp\left[\frac{1}{k_BT\Omega_s}\left(-\varepsilon_1 + \eta\frac{\gamma_1}{L_1}\right)\right]$ and $c_{2-} = c_{ref}\exp\left[\frac{1}{k_BT\Omega_s}\left(\varepsilon_1 - \varepsilon_2 + \eta\frac{\gamma_2}{L_2}\right)\right]$, respectively. The growth of layer 2 simply requires that $c_{1-} > c_{2-}$. Therefore, the size-dependent thermodynamic criterion for vertical growth can be written as

$$\Delta\varepsilon_{bind} = \varepsilon_{LL} - \varepsilon_{L1S} > \eta(\gamma_2/L_2 - \gamma_1/L_1) \quad (6)$$

where ε_{LL} is the vdW binding energy density between two layers and ε_{L1S} is the binding energy density between layer 1 and the substrate. The difference between these two energies, $\Delta\varepsilon_{bind}$, gives the energy gain of adding atoms to the subsequent layer instead of lateral monolayer growth of the existing layer. Figure 3(a) expands on the thermodynamic growth criterion in eq 6 and shows how $\Delta\varepsilon_{bind}$ must be of sufficient value to overcome the energy penalty of increasing the layer perimeter. The vertical bilayer growth criterion becomes easier to meet as ε_{L1S} decreases toward the freestanding case of $\varepsilon_{L1S} = 0$, and this is qualitatively consistent with previous thermodynamic analysis.[30] The left-hand side of eq 6 can be modified to account for alternative layer growth mechanisms; for example, for bilayer graphene on a Cu(111) surface where layer 2 lies between layer 1 and the substrate,[31] $\Delta\varepsilon_{bind}$ should be modified as $\Delta\varepsilon_{bind} = \varepsilon_{LL} + \varepsilon_{L2S} - 2\varepsilon_{L1S}$, where ε_{L2S} is the vdW binding energy density between layer 2 and the substrate. The $\Delta\varepsilon_{bind}$ and γ are constant for a given material and substrate system, and from these values the previously discussed size limits L_{1max} and L_{2min} for layer 2 growth can be quantitatively determined *via* eq 6. A heat map is given in Figure 3(b) showing the minimum requirements of material properties $\Delta\varepsilon_{bind}$, γ, and η for layer 2 growth at certain sizes of layer 1 and layer 2, assuming γ is equivalent for both layers. The black solid lines with open symbols in Figure 3(b) are obtained by numerically scanning over the size limit L_{1max}, and these results are consistent with the heat map contours established by eq 6. The

DOI: 10.1021/acsnano.7b07604
ACS Nano 2017, 11, 12780−12788

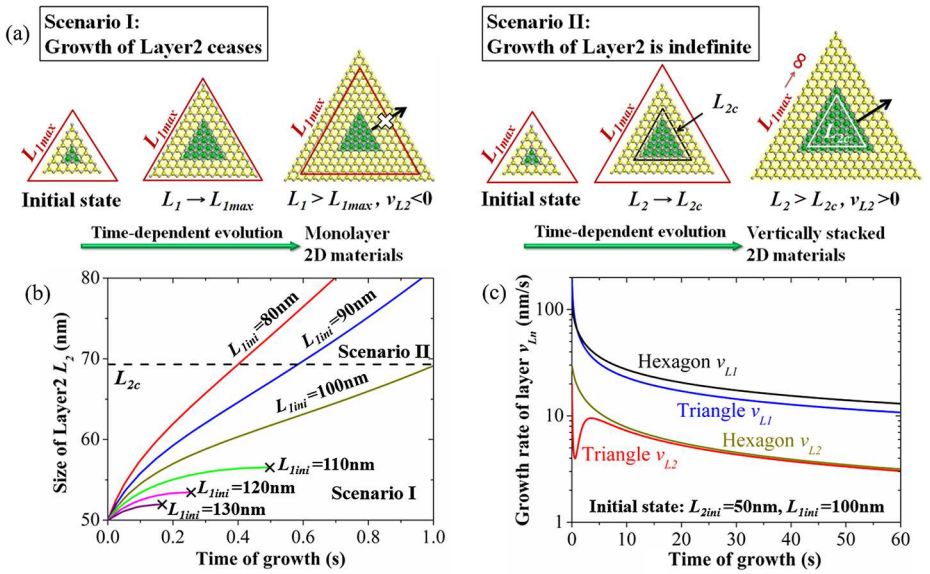

Figure 4. (a) Schematic representations of two scenarios of time-dependent layer growth. (b) Time-dependent size of layer 2 at varying initial sizes of layer 1 beginning with L_{2ini} = 50 nm. (c) Individual layer growth rate as a function of time for vertically stacked layers of triangular and hexagonal shapes.

discrepancy in L_{1max} for hexagonal and triangular layers of identical material arises from the difference in the structural parameter η. At a critical size of layer 2 (L_{2c}), the L_{1max} rises rapidly to infinity. While the growth rate still depends on the instantaneous L_1 and L_2, beyond L_{2c} the positive growth of layer 2 will proceed regardless of the size of layer 1. This L_{2c} value follows an inverse relation to $\Delta\varepsilon_{bind}/(\eta\gamma)$.

The absolute growth rate of layer 2 strongly relates to the parameters adopted in the diffusion model, specifically F, K_+, and λ. The flux F accounts for the supply of adatom on the substrate, the kinetic coefficient K_+ provides an estimate for the ability of adatoms to hop from the substrate to layer 1, and the diffusion length λ describes the effective distance an atom can move during its adsorbed lifetime. In Figure 3(c), we numerically scan these parameters to determine their influence on the growth rate using a triangular model system with a fixed L_2 of 50 nm. Increasing any of these parameters will enhance the absolute growth rate of layer 2. However, the crossover point v_{L2} = 0 and corresponding size limit L_{1max} do not change, indicating that the simple thermodynamic growth criterion established by eq 6 remains valid. Although these growth parameters are experimentally accessible (*e.g.*, by gas flow and temperature), they are not able to adjust the layer 2 growth criterion at certain layer sizes. To further investigate the issue of relevant experimental controls, we next consider the time-dependent growth process.

Initial Layer Sizes, Temperature, and Adatom Flux from Vapor Are the Primary Criteria Affecting the Final Structure in Time-Dependent Growth. Two distinct scenarios emerge when time dependence is considered in the growth of vertically stacked 2D materials, as depicted in Figure 4(a). In both cases, the initial state consists of two layers obeying the criterion for layer 2 growth ($L_2 > L_{2min}$ and $L_1 < L_{1max}$). In scenario I, L_1 approaches and exceeds L_{1max} after some time. Consequently, the size of layer 1 prohibits further layer 2 growth and layer 2 will prefer to shrink. The final structure of scenario I will be just the monolayer, since the lateral in-plane growth of layer 1 dominates. Scenario II begins similarly, but in this case L_2 exceeds L_{2c} before L_1 can reach L_{1max}, with the result that layer 2 will continue to grow at a positive rate indefinitely, leading to a vertically stacked structure. Clearly, the resulting structure depends on the kinetic competition between the sizes of layer 1 and layer 2, subject to the thermodynamic parameters of the material system. These requirements apply in addition to the criterion established in eq 6, which is only instantaneously valid for given sizes of layer 1 and layer 2.

Figure 4(b) shows that the initial state strongly affects the growth mode and growth rate. From the thermodynamic analysis, the critical size for stability of bilayer TMDs is on the order of tens of nanometers.[30] Since the final layer size is on the order of micrometers,[26−28] we measure the layer growth from an initial L_2 of 50 nm as an illustrative case. The detailed nucleation process of layer 2 beginning with only several adatoms and the related nucleation probability[32] are not considered. In all quasi-static simulations, the diameter of the substrate is set to 20 μm. For triangular shape, the corresponding maximum size of layer 1 (L_{1max}) and the critical size of layer 2 (L_{2c}) are 179.7 nm and 69.3 nm, respectively. As illustrated in Figure 4(b), layer 2 growth ceases at only 0.17, 0.26, and 0.5 s when the initial size of layer 1 (L_{1ini}) is 130, 120, and 110 nm, respectively. However, the growth of layer 2 will proceed indefinitely if $L_{1ini} \leq$ 100 nm. Mechanistically, this arises from the fact that increasing L_{1ini} decreases the growth rate of layer 2 (v_{L2}), allowing layer 1 to reach L_{1max} with ease.

Next, we investigate a case of successful vertical growth with initial conditions L_{2ini} = 50 nm and L_{1ini} = 100 nm. The time-dependent growth rates of vertically stacked layers with triangular and hexagonal shapes are plotted in Figure 4(c). After 60 s, L_1 and L_2 for the triangular shape reach 3954 and 1079 nm, respectively, while the values for the hexagonal shape are roughly half these at 1583 and 454 nm (see Supporting Information, Figure S1). Generally, layer 1 grows faster than layer 2 and the growth rates of both layers decrease over time. The clear dip of v_{L2} in the triangular model is due to L_1 approaching L_{1max} in the early stage of growth; if v_{L2} had continued to drop and gone below zero, the growth mode would fall into scenario I. This dip is not observed in the

DOI: 10.1021/acsnano.7b07604
ACS Nano 2017, 11, 12780−12788

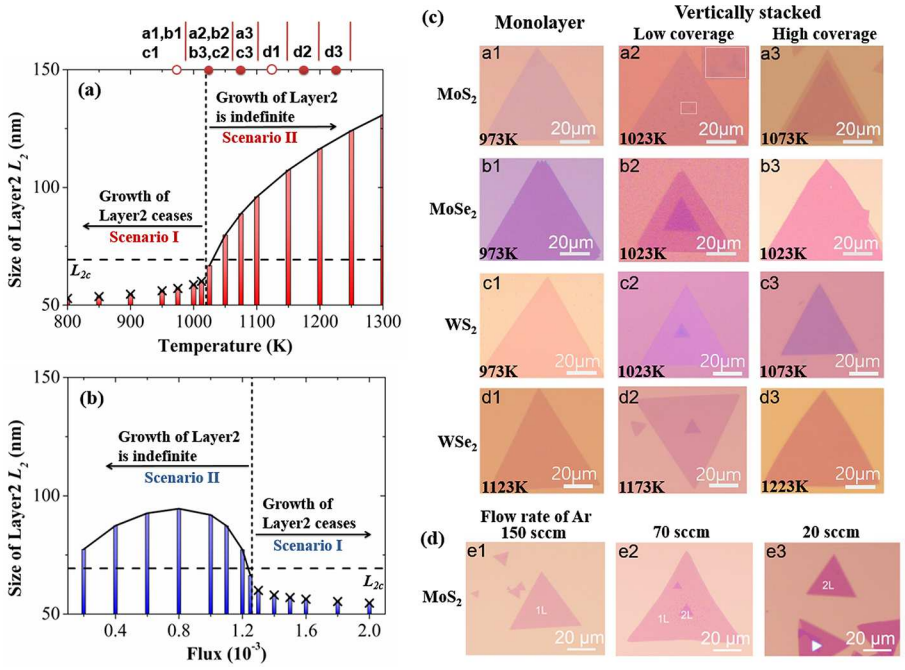

Figure 5. (a) Influence of temperature on the growth of layer 2. (b) Influence of flux (unit Ω_s) on the growth of layer 2. The growth time of the successful vertical growth connected with the solid line is 2 s. (c) Optical images of TMD samples grown by CVD at different temperatures, including monolayer and vertically stacked bilayer MoS_2 (a1 to a3), $MoSe_2$ (b1 to b3), WS_2 (c1 to c3), and WSe_2 (d1 to d3). The corresponding growth temperatures of samples are marked in (a). (d) Optical images of MoS_2 samples grown at 1023 K under different fluxes (e1 to e3). The flow rate of Ar is 150, 70, and 20 sccm, respectively.

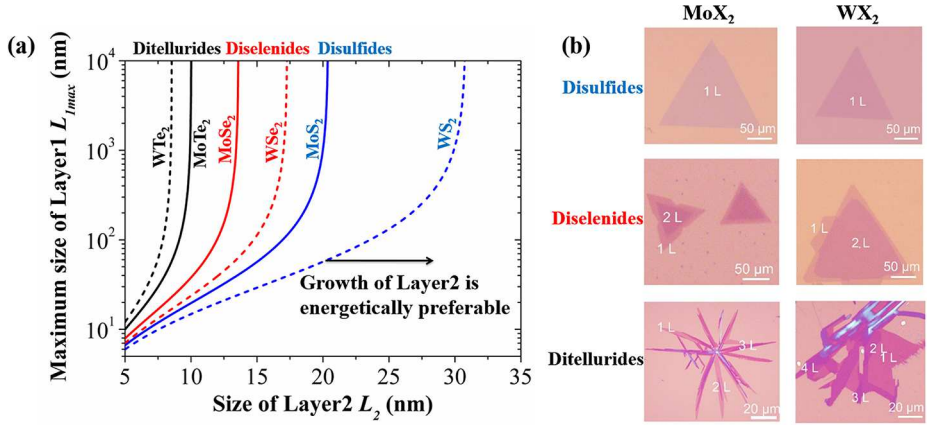

Figure 6. (a) Dependence of the maximum size of layer 1 on size of layer 2 for MX_2 (M = Mo, W; X = S, Se, Te). (b) Optical images of MX_2 (M = Mo, W; X = S, Se, Te), showing increased layer stacking moving down the chalcogenide period. The growth conditions are as follows: MoS_2, 1023 K, 15 min; $MoSe_2$, 1023 K, 15 min; $MoTe_2$, 973 K, 5 min; WS_2, 1023 K, 15 min; WSe_2, 1123 K, 10 min; WTe_2, 1103 K, 5 min.

hexagonal model because the example L_{2ini} (50 nm) is already larger than the corresponding L_{2c} (23.1 nm).

As previously discussed, the time-dependent growth process establishes the connection between experimentally observed growth conditions for vertically stacked 2D materials and the proposed growth model. Using the same initial conditions of L_{2ini} = 50 nm and L_{1ini} = 100 nm, we first examine the effect of growth temperature. The temperature may modify both diffusion coefficient D and kinetic coefficient K, which are considered separately. First, we have verified that the growth mode is not sensitive to changing only the diffusion coefficient among the default parameters within an order of magnitude larger or smaller; this merely varies the absolute growth rates. For the kinetic coefficient K, the influence of the temperature is captured by the ratio of K_+ to K_-, which is given by the relation $K_{n+} = K_{n-} \exp(-V_b/k_BT)$,[32] where V_b is the energy barrier an adatom must overcome to hop from domain $n-1$ to domain n. The value of V_b is chosen to be 0.23 eV, consistent with ref 32. At higher temperature, K_+ approaches K_-, indicating that more adatoms will climb from the substrate to layer 1, where they will have a chance to contribute to vertical growth. Figure 5(a) shows a critical temperature T_c of 1020 K for indefinite layer 2 growth. Below this critical temperature, the layer 2 growth ceases in the early stage and growth of layer 1 prevails, corresponding with scenario I discussed earlier. Otherwise, growth of the stacked layers remains favorable. In order to verify the predicted trend, we synthesize MX_2 (M = Mo, W; X = S, Se) *via* CVD at different temperatures. The optical images of final structures are shown in Figure 5(c). The monolayers are observed at low growth temperatures (*e.g.*, MoS_2, $MoSe_2$,

DOI: 10.1021/acsnano.7b07604
ACS Nano 2017, 11, 12780−12788

and WS_2 at 973 K), while the vertically stacked bilayer structures are obtained at high temperatures (*e.g.*, MoS_2, $MoSe_2$, and WS_2 at 1023 K). Further increasing the temperature clearly increases the layer 2 coverage in the final structure, indicating the ease of layer 2 growth. In contrast to disulfides and diselenides, bilayer and few-layer ditellurides can be easily produced at the same growth temperature (see Supporting Information, Figure S2). When considering WS_2/MoS_2 heterostructures,[26] which have been reported to grow laterally (monolayer) at 923 K and vertically (stacked bilayer) at 1123 K, the predicted trend of temperature on growth mode works as well.

In addition to temperature, we examine the effect of flux, which can be controlled by the gas flow rate in CVD. As illustrated in Figure 5(b) (calculated with the default parameter set), a critical flux $F_c = 1.26 \times 10^{-3}\Omega_s$ exists, below which growth of stacked layers is ensured. Qualitatively, decreasing the supply of adatoms on the substrate benefits vertical growth, which agrees with the reported experimental observations of bilayer graphene.[34] Figure 5(d) demonstrates the MoS_2 samples grown isothermally at 1023 K under different flow rates of argon gas. Monolayer MoS_2, bilayer MoS_2 with low layer 2 coverage, and bilayer MoS_2 with high layer 2 coverage are respectively observed at 150, 70, and 20 sccm. This behavior is consistent with our predicted trend of flux on the growth mode.

The Thermodynamic Criterion Coupled with DFT-Calculated Energies Can Predict the Ease of Fabrication for Vertically Stacked TMDs: Ditellurides > Diselenides > Disulfides. Finally, we quantitatively evaluate the size limits for vertical growth of specific TMDs by incorporating the energies from DFT calculations into the thermodynamic criterion. The calculated edge energy densities and vdW interaction energy densities (between two layers and between layer and SiO_2 substrate) of TMDs are listed in Table S1. The maximum sizes of the initial layer as a function of layer 2 size for MX_2 (M = Mo, W; X = S, Se, Te) are plotted in Figure 6(a). Layer 2 growth is energetically preferable when the sizes of layer 1 and layer 2 fall below the lines for the corresponding TMDs. The critical sizes of layer 2 (L_{2c}) for indefinite vertical growth are 20.2, 13.6, and 10.0 nm for MoS_2, $MoSe_2$, and $MoTe_2$, respectively, while the corresponding tungsten dichalcogenide values are 30.8, 17.3, and 8.5 nm. With a lower L_{2c}, it is easier to achieve the scenario II growth mode, which favors vertically stacked structures as the final product in the time-dependent process. Therefore, the probability for a successfully nucleated vertical island to achieve this stable growth mode increases from disulfides to diselenides to ditellurides in the TMD material family. This predicted trend is validated by the synthesized structures of MX_2 shown in Figure 6(b). The optical images clearly show an increasing number of vertical layers with X moving down the chalcogenide period. Similar behavior is also observed for niobium dichalcogenides (see Supporting Information, Figure S3). Using more reliable measured or calculated parameters for materials of interest, the proposed model can provide further predictions to guide fabrication of vertically stacked 2D materials.

CONCLUSIONS

In this work, we have proposed a general growth model for vertically stacked 2D materials, identifying the physical parameters that play important roles in determining the final structure. First, the growth rate of layer 2 is found to strongly depend on the instantaneous sizes of layer 1 and layer 2. A material-dependent maximum size of layer 1 (L_{1max}) and minimum size of layer 2 (L_{2min}) bound the positive growth ($v_{L2} > 0$) region for layer 2. Next, an analytic thermodynamic criterion for layer 2 growth is obtained, and we find that beyond a critical layer 2 size (L_{2c}), the layer 2 growth becomes indefinite regardless of layer 1 size. The experimentally relevant environmental parameters do not affect this analytic criterion, but play crucial roles in the time-dependent growth process by controlling the transport of adatoms within and between the layers. Using quasi-static simulations, we find that temperature, adatom flux from vapor, and initial layer sizes control the final structure due to the specific evolution of layer 1 and layer 2 in the early stage of growth. Finally, based on the energies from DFT calculations, bilayer TMDs can be most readily synthesized in the case of ditellurides followed by diselenides and disulfides. The experimental observations of CVD-grown monolayer and vertically stacked bilayer MX_2 (M = Mo, W; X = S, Se, Te) verify the influence of temperature and flux on the final structure and show increasing number of layers with X moving down the chalcogenide period, which are consistent with the predictions from the proposed model. With this improved mechanistic understanding, we believe this model can guide future efforts toward CVD fabrication of vertically stacked 2D materials.

METHODS

Simulation of Layer Growth. The growth of vertically stacked 2D materials is investigated by constructing the diffusion equations with flux boundary conditions that are derived from the mass conservation and the second law of thermodynamics ensuring the reduction of total free energy during growth. The steady-state diffusion equations are solved by the finite element method (FEM). When simulating the time-dependent growth process, we adopt the quasi-static approach in which steady-state growth rates are applied as normal boundary velocities of 2D layers by adopting the arbitrary Lagrangian−Eulerian (ALE)[36] formulation in FEM. The diffusion equations are solved with updated geometry in the next time iteration.[37]

DFT Calculations. All DFT calculations are performed using the VASP package[38] with the projector augmented wave (PAW)[39−41] potentials for core electrons and the Perdew−Burke−Ernzerhof (PBE)[42] form of the generalized gradient approximation (GGA) for the exchange and correlation functional. An energy cutoff of 520 eV is used for the plane-wave basis expansion. The unit cells of monolayer MX_2 (M = Mo, W; X = S, Se, Te) are relaxed with a Γ-centered *k*-point mesh of 12 × 12 × 1 in the first Brillouin zone. The supercells for freestanding bilayers (AB stacking) and monolayers on the α-quartz (SiO_2) substrate are relaxed with a Γ-centered *k*-point mesh of 4 × 4 × 1. Both structures are converged with an energy difference below 10^{-7} eV. To capture the vdW interactions between two TMD layers and between the TMD layer and the α-quartz substrate, we applied the DFT-D2 functional, which adds a pairwise force field to the conventional Kohn−Sham DFT energy.[43,44] Additional details can be found in the Supporting Information.

Preparation of TMD Samples. (1) Synthesis of MoS_2: MoS_2 is grown *via* CVD under atmospheric pressure. In a typical growth, MoO_3 powder (1 mg) in an alumina boat is located at the middle of a tube furnace, while sulfur elemental powder (1 g) in another alumina boat is upwind of the MoO_3. A piece of Si wafer with 280 nm SiO_2 top layer is suspended on the MoO_3 boat with the polished surface down. Argon gas of 100 standard cubic centimeters per minute (sccm) is used as carrier gas and provides an inert atmosphere as well. The system is heated to growth temperatures with a heating rate of 50 K/min. After the system is maintained at the growth temperature for 15 min while the sulfur is fixed at 470 K, the system is then cooled naturally. (2) Synthesis of $MoSe_2$: The method is analogous to the

DOI: 10.1021/acsnano.7b07604
ACS Nano 2017, 11, 12780−12788

growth of MoS_2 while the selenium is fixed at 570 K and the mixed gas of Ar/H_2 with a flow rate of 70/5 sccm is used as carrier gas. (3) Synthesis of $MoTe_2$: The method is similar to the reported results in ref 45. (4) Synthesis of WS_2: The method is analogous to the growth of MoS_2, but changing the MoO_3 to WO_3. (5) Synthesis of WSe_2: The growth method can be found elsewhere.[46] (6) Synthesis of WTe_2: The method is similar to the reported results in ref 45. (7) Synthesis of $NbS_2/NbSe_2/NbTe_2$: Mixed powder of NaCl and Nb_2O_5 with weights of 1 mg and 6 mg in an alumina boat is placed in the center of the tube. Another alumina boat containing S/Se/Te powder is placed upstream with the temperature of 470, 570, and 670 K, respectively. The furnace is heated with a ramp rate of 50 K/min to the growth temperatures and held at this temperature for 5 min before being cooled to room temperature naturally. Ar/H_2 with a flow rate of 80/10 sccm is used as carrier gas.

ASSOCIATED CONTENT

Supporting Information

The Supporting Information is available free of charge on the ACS Publications website at DOI: 10.1021/acsnano.7b07604.

Size evolution of vertically stacked layers with time; optical images of $MoTe_2$ and WTe_2 samples; optical images of NbS_2, $NbSe_2$, and $NbTe_2$ samples; summary of energies from DFT calculations; detailed derivations of the governing equations; additional details of DFT calculations (PDF)

AUTHOR INFORMATION

Corresponding Author

*E-mail: vshenoy@seas.upenn.edu.

ORCID

Han Ye: 0000-0002-9119-4781

Zheng Liu: 0000-0002-8825-7198

Notes

The authors declare no competing financial interest.

ACKNOWLEDGMENTS

The work is supported primarily by contract W911NF-16-1-0447 from the Army Research Office (V.B.S.) and also by grants EFMA-542879 (D.E.), CMMI-1727717 (C.P.), and DMS-1522603 from the U.S. National Science Foundation. H.Y. thanks the support from the National Natural Science Foundation of China (NSFC) (61401035, 61671090) and Fund of State Key Laboratory of Information Photonics and Optical Communications (Beijing University of Posts and Telecommunications), P. R. China (IPOC2017ZT07). This work is also supported by the Singapore National Research Foundation under NRF RF Award No. NRF-RF2013-08, Tier 2 MOE2016-T2-2-153, and MOE2015-T2-2-007.

REFERENCES

(1) Zhang, Y. B.; Tan, Y. W.; Stormer, H. L.; Kim, P. Experimental Observation of the Quantum Hall Effect and Berry's Phase in Grapheme. *Nature* **2005**, *438*, 201−204.

(2) Das, A.; Pisana, S.; Chakraborty, B.; Piscanec, S.; Saha, S. K.; Waghmare, U. V.; Novoselov, K. S.; Krishnamurthy, H. R.; Geim, A. K.; Ferrari, A. C.; Sood, A. K. Monitoring Dopants by Raman Scattering in an Electrochemically Top-Gated Graphene Transistor. *Nat. Nanotechnol.* **2008**, *3*, 210−215.

(3) Novoselov, K. S.; Geim, A. K.; Morozov, S. V.; Jiang, D.; Zhang, Y.; Dubonos, S. V.; Grigorieva, I. V.; Firsov, A. A. Electric Field Effect in Atomically Thin Carbon Films. *Science* **2004**, *306*, 666−669.

(4) Li, L. L.; Yu, Y. J.; Ye, G. J.; Ge, Q. Q.; Ou, X. D.; Wu, H.; Feng, D. L.; Chen, X. H.; Zhang, Y. B. Black Phosphorus Field-Effect Transistors. *Nat. Nanotechnol.* **2014**, *9*, 372−377.

(5) Kamal, C.; Ezawa, M. Arsenene: Two-Dimensional Buckled and Puckered Honeycomb Arsenic Systems. *Phys. Rev. B: Condens. Matter Mater. Phys.* **2015**, *91*, 085423.

(6) Nag, A.; Raidongia, K.; Hembram, K. P.; Datta, R.; Waghmare, U. V.; Rao, C. N. R. Graphene Analogues of BN: Novel Synthesis and Properties. *ACS Nano* **2010**, *4*, 1539−1544.

(7) Kim, K. K.; Hsu, A.; Jia, X. T.; Kim, S. M.; Shi, Y. M.; Hofmann, M.; Nezich, D.; Rodriguez-Nieva, J. F.; Dresselhaus, M.; Palacios, T.; Kong, J. Synthesis of Monolayer Hexagonal Boron Nitride on Cu Foil Using Chemical Vapor Deposition. *Nano Lett.* **2012**, *12*, 161−166.

(8) Xiao, D.; Liu, G. B.; Feng, W. X.; Xu, X. D.; Yao, W. Coupled Spin and Valley Physics in Monolayers of MoS_2 and Other Group-VI Dichalcogenides. *Phys. Rev. Lett.* **2012**, *108*, 196802.

(9) Radisavljevic, B.; Radenovic, A.; Brivio, J.; Giacometti, V.; Kis, A. Single-Layer MoS_2 Transistors. *Nat. Nanotechnol.* **2011**, *6*, 147−150.

(10) He, Y. M.; Clark, G.; Schaibley, J. R.; He, Y.; Chen, M. C.; Wei, Y. J.; Ding, X.; Zhang, Q.; Yao, W.; Xu, X. D.; Lu, C. Y.; Pan, J. W. Single Quantum Emitters in Monolayer Semiconductors. *Nat. Nanotechnol.* **2015**, *10*, 497−502.

(11) Ramasubramaniam, A.; Naveh, D.; Towe, E. Tunable Band Gaps in Bilayer Transition-Metal Dichalcogenides. *Phys. Rev. B: Condens. Matter Mater. Phys.* **2011**, *84*, 205325.

(12) Puretzky, A. A.; Liang, L. L.; Li, X. F.; Xiao, K.; Sumpter, B. G.; Meunier, V.; Geohegan, D. B. Twisted $MoSe_2$ Bilayers with Variable Local Stacking and Interlayer Coupling Revealed by Low-Frequency Raman Spectroscopy. *ACS Nano* **2016**, *10*, 2736−2744.

(13) Park, S.; Kim, H.; Kim, M. S.; Han, G. H.; Kim, J. Dependence of Raman and Absorption Spectra of Stacked Bilayer MoS_2 on the Stacking Orientation. Opt. *Opt. Express* **2016**, *24*, 21551.

(14) Ohta, T.; Bostwick, A.; Seyller, T.; Horn, K.; Rotenberg, E. Controlling the Electronic Structure of Bilayer Graphene. *Science* **2006**, *313*, 951−954.

(15) Zhang, Y. B.; Tang, T. T.; Girit, C.; Hao, Z.; Martin, M. C.; Zettl, A.; Crommie, M. F.; Shen, Y. R.; Wang, F. Direct Observation of a Widely Tunable Bandgap in Bilayer Graphene. *Nature* **2009**, *459*, 820−823.

(16) Castro, E. V.; Novoselov, K. S.; Morozov, S. V.; Peres, N. M. R.; Dos Santos, J. M. B.; Nilsson, J.; Guinea, F.; Geim, A. K.; Neto, A. H. C. Biased Bilayer Graphene: Semiconductor with a Gap Tunable by the Electric Field Effect. *Phys. Rev. Lett.* **2007**, *99*, 216802.

(17) Lee, C. H.; Lee, G. H.; Van Der Zande, A. M.; Chen, W. C.; Li, Y. L.; Han, M. Y.; Cui, X.; Arefe, G.; Nuckolls, C.; Heinz, T. F.; Guo, J.; Hone, J.; Kim, P. Atomically Thin P-N Junctions with van Der Waals Heterointerfaces. *Nat. Nanotechnol.* **2014**, *9*, 676−681.

(18) Fang, H.; Battaglia, C.; Carraro, C.; Nemsak, S.; Ozdol, B.; Kang, J. S.; Bechtel, H. A.; Desai, S. B.; Kronast, F.; Unal, A. A.; Conti, G.; Conlon, C.; Palsson, G. K.; Martin, M. C.; Minor, A. M.; Fadley, C. S.; Yablonovitch, E.; Maboudian, R.; Javey, A. Strong Interlayer Coupling in van Der Waals Heterostructures Built from Single-Layer Chalcogenides. Proc. *Proc. Natl. Acad. Sci. U. S. A.* **2014**, *111*, 6198−6202.

(19) Rivera, P.; Schaibley, J. R.; Jones, A. M.; Ross, J. S.; Wu, S. F.; Aivazian, G.; Klement, P.; Seyler, K.; Clark, G.; Ghimire, N. J.; Yan, J. Q.; Mandrus, D. G.; Yao, W.; Xu, X. D. Observation of Long-Lived Interlayer Excitons in Monolayer $MoSe_2$-WSe_2 Heterostructures. *Nat. Commun.* **2015**, *6*, 6242.

(20) Heo, H.; Sung, J. H.; Cha, S.; Jang, B. G.; Kim, J. Y.; Jin, G.; Lee, D.; Ahn, J. H.; Lee, M. J.; Shim, J. H.; Choi, H.; Jo, M. H. Interlayer Orientation-Dependent Light Absorption and Emission in Monolayer Semiconductor Stacks. *Nat. Commun.* **2015**, *6*, 7372.

(21) Hong, X. P.; Kim, J.; Shi, S. F.; Zhang, Y.; Jin, C. H.; Sun, Y. H.; Tongay, S.; Wu, J. Q.; Zhang, Y. F.; Wang, F. Ultrafast Charge Transfer in Atomically Thin MoS_2/WS_2 Heterostructures. *Nat. Nanotechnol.* **2014**, *9*, 682−686.

(22) Rigosi, A. F.; Hill, H. M.; Li, Y. L.; Chernikov, A.; Heinz, T. F. Probing Interlayer Interactions in Transition Metal Dichalcogenide

DOI: 10.1021/acsnano.7b07604
ACS Nano 2017, 11, 12780−12788

Heterostructures by Optical Spectroscopy: MoS_2/WS_2 and $MoSe_2/WSe_2$. *Nano Lett.* **2015**, *15*, 5033−5038.
(23) Ceballos, F.; Bellus, M. Z.; Chiu, H. Y.; Zhao, H. Ultrafast Charge Separation and Indirect Exciton Formation in a MoS_2-$MoSe_2$ van Der Waals Heterostructure. *ACS Nano* **2014**, *8*, 12717−12724.
(24) Yu, Y. F.; Hu, S.; Su, L. Q.; Huang, L. J.; Liu, Y.; Jin, Z. H.; Puretzky, A. A.; Geohegan, D. B.; Kim, K. W.; Zhang, Y.; Cao, L. Y. Equally Efficient Inter-Layer Exciton Relaxation and Improved Absorption in Epitaxial and Nonepitaxial MoS_2/WS_2 Heterostructures. *Nano Lett.* **2015**, *15*, 486−491.
(25) Chu, T.; Ilatikhameneh, H.; Klimeck, G.; Rahman, R.; Chen, Z. H. Electrically Tunable Bandgaps in Bilayer MoS_2. *Nano Lett.* **2015**, *15*, 8000−8007.
(26) Gong, Y. J.; Lin, J. H.; Wang, X. L.; Shi, G.; Lei, S. D.; Lin, Z.; Zou, X. L.; Ye, G. L.; Vajtai, R.; Yakobson, B. I.; Terrones, H.; Terrones, M.; Tay, B. K.; Lou, J.; Pantelides, S. T.; Liu, Z.; Zhou, W.; Ajayan, P. M. Vertical and In-Plane Heterostructures from WS_2/MoS_2 Monolayers. *Nat. Mater.* **2014**, *13*, 1135−1142.
(27) Xia, M.; Li, B.; Yin, K.; Capellini, G.; Niu, G.; Gong, Y. J.; Zhou, W.; Ajayan, P. M.; Xie, Y. H. Spectroscopic Signatures of AA' and AB Stacking of Chemical Vapor Deposited Bilayer MoS_2. *ACS Nano* **2015**, *9*, 12246−12254.
(28) Gong, Y. J.; Lei, S. D.; Ye, G. L.; Li, B.; He, Y. M.; Keyshar, K.; Zhang, X.; Wang, Q. Z.; Lou, J.; Liu, Z.; Vajtai, R.; Zhou, W.; Ajayan, P. M. Two-Step Growth of Two-Dimensional $WSe_2/MoSe_2$ Heterostructures. *Nano Lett.* **2015**, *15*, 6135−6141.
(29) He, J. G.; Hummer, K.; Franchini, C. Stacking Effects on the Electronic and Optical Properties of Bilayer Transition Metal Dichalcogenides MoS_2, $MoSe_2$, WS_2, and WSe_2. *Phys. Rev. B: Condens. Matter Mater. Phys.* **2014**, *89*, 075409.
(30) Shang, S. L.; Lindwall, G.; Wang, Y.; Redwing, J. M.; Anderson, T.; Liu, Z. K. Lateral *versus* Vertical Growth of Two-Dimensional Layered Transition-Metal Dichalcogenides: Thermodynamic Insight into MoS_2. *Nano Lett.* **2016**, *16*, 5742−5750.
(31) Ta, H. Q.; Perello, D. J.; Duong, D. L.; Han, G. H.; Gorantla, S.; Nguyen, V. L.; Bachmatiuk, A.; Rotkin, S. V.; Lee, Y. H.; Rümmeli, M. H. Stranski−Krastanov and Volmer-Weber CVD Growth Regimes to Control the Stacking Order in Bilayer Graphene. *Nano Lett.* **2016**, *16*, 6403−6410.
(32) Chen, W.; Cui, P.; Zhu, W. G.; Kaxiras, E.; Gao, Y. F.; Zhang, Z. Y. Atomistic Mechanisms for Bilayer Growth of Graphene on Metal Substrates. *Phys. Rev. B: Condens. Matter Mater. Phys.* **2015**, *91*, 045408.
(33) Zhang, X. Y.; Wang, L.; Xin, J.; Yakobson, B. I.; Ding, F. Role of Hydrogen in Graphene Chemical Vapor Deposition Growth on a Copper Surface. *J. Am. Chem. Soc.* **2014**, *136*, 3040−3047.
(34) Xing, S. R.; Wu, W.; Wang, Y.; Bao, J. M.; Pei, S. S. Kinetic Study of Graphene Growth: Temperature Perspective on Growth Rate and Film Thickness by Chemical Vapor Deposition. *Chem. Phys. Lett.* **2013**, *580*, 62−66.
(35) Rajan, A. G.; Warner, J. H.; Blankschtein, D.; Strano, M. S. Generalized Mechanistic Model for the Chemical Vapor Deposition of 2D Transition Metal Dichalcogenide Monolayers. *ACS Nano* **2016**, *10*, 4330−4344.
(36) Donea, J.; Huerta, A.; Ponthot, J. P.; Rodrıgues-Ferran, A. Arbitrary Langrangian-Eulerian methods. In *Encyclopedia of Computational Mechanics*; Stein, E., De Borst, R., Hughes, T. J. R., Eds.; John Wiley & Sons, 2004; pp 1−25.
(37) Ye, H.; Yu, Z. Y.; Kodambaka, S.; Shenoy, V. B. Kinetics of Axial Composition Evolution in Multi-component Alloy Nanowires. *Appl. Phys. Lett.* **2012**, *100*, 263103.
(38) Kresse, G.; Hafner, J. Ab Initio Molecular Dynamics for Liquid Metals. *Phys. Rev. B: Condens. Matter Mater. Phys.* **1993**, *47*, 558−561.
(39) Kresse, G.; Furthmüller, J. Efficiency of Ab-Initio Total Energy Calculations for Metals and Semiconductors Using a Plane-Wave Basis Set. *Comput. Mater. Sci.* **1996**, *6*, 15−50.
(40) Kresse, G.; Hafner, J. Ab Initio Molecular-Dynamics Simulation of the Liquid-Metal−amorphous-Semiconductor Transition in Germanium. *Phys. Rev. B: Condens. Matter Mater. Phys.* **1994**, *49*, 14251−14269.
(41) Kresse, G.; Furthmüller, J. Efficient Iterative Schemes for Ab Initio Total-Energy Calculations Using a Plane-Wave Basis Set. *Phys. Rev. B: Condens. Matter Mater. Phys.* **1996**, *54*, 11169−11186.
(42) Perdew, J.; Burke, K.; Ernzerhof, M. Generalized Gradient Approximation Made Simple. *Phys. Rev. Lett.* **1996**, *77*, 3865−3868.
(43) Grimme, S.; Diedrich, C.; Korth, M. The Importance of Inter- and Intramolecular van Der Waals Interactions in Organic Reactions: The Dimerization of Anthracene Revisited. *Angew. Chem., Int. Ed.* **2006**, *45*, 625−629.
(44) Harl, J.; Schimka, L.; Kresse, G. Assessing the Quality of the Random Phase Approximation for Lattice Constants and Atomization Energies of Solids. *Phys. Rev. B: Condens. Matter Mater. Phys.* **2010**, *81*, 115126.
(45) Zhou, J. D.; Liu, F. C.; Lin, J. H.; Huang, X. W.; Xia, J.; Zhang, B. W.; Zeng, Q. S.; Wang, H.; Zhu, C.; Niu, L.; Wang, X. W.; Fu, W.; Yu, P.; Chang, T. R.; Hsu, C. H.; Wu, D.; Jeng, H. T.; Huang, Y. Z.; Lin, H.; Shen, Z. X.; et al. Large-Area and High-Quality 2D Transition Metal Telluride. *Adv. Mater.* **2017**, *29*, 1603471.
(46) Gong, Y. J.; Ye, G.; Lei, S.; Shi, G.; He, Y.; Lin, J.; Zhang, X.; Vajtai, R.; Pantelides, S. T.; Zhou, W.; Li, B.; Ajayan, P. M. Synthesis of Millimeter-Scale Transition Metal Dichalcogenides Single Crystals. *Adv. Funct. Mater.* **2016**, *26*, 2009−2015.

DOI: 10.1021/acsnano.7b07604
ACS Nano 2017, 11, 12780−12788